Materials Research, Vol. 11, No. 3, 289-293, 2008

Kinetic Study of α-BZN Crystallization Obtained from Chemical Method

Ronaldo Rodrigues Pelá[a], *Luciana Simone Cividanes*[a], *Deborah Dibbern Brunelli*[a], *Sonia Maria Zanetti*[b], *Gilmar Patrocinio Thim*[a]*

[a]*Departamento de Química, Instituto Tecnológico de Aeronáutica, Pça. Marechal Eduardo Gomes, 50, Vila das Acácias, 12298-900 São José dos Campos - SP, Brazil*
[b]*Laboratório Associado de Sensores e Materiais, Instituto Nacional de Pesquisas Espaciais, Av. dos Astronautas, 1758, Jd. da Granja, 12227-010 São José dos Campos - SP, Brazil*

Received: March 5, 2008; Revised: August 11, 2008

The crystallization kinetics of ceramics composed by Bi_2O_3-ZnO-Nb_2O_5 (BZN) was studied using non-isothermal method. The BZN samples were prepared by the polymeric precursors method. Phase evolution was evaluated by X ray diffraction and the thermal events were evaluated by differential scanning calorimetry (DSC). The crystallization of BZN occurs from 500 to 700 °C, which corresponds to a secondary event in DSC curves. The principal exothermic event in these curves is related to the decomposition of organic material and was isolated from the crystallization peak by deconvolution into two Gaussian curves. Those related to crystallization processes were evaluated in terms of crystallized fraction. Kinetic parameters were determined from Ligero ($E = 242 \pm 7$) kJ.mol^{-1} and Kissinger ($E = 241 \pm 24$) kJ.mol^{-1} methodologies and they are very close. The activation energy Ea = (241 ± 24) kJ.mol^{-1} and (242 ± 7) kJ.mol^{-1} (by the Kissinger and Ligero methodology, respectively), frequency factor $k_0 = 10^{13}.s^{-1}$ and exponent of Avrami $n = (1.3 \pm 0.1)$ were determined. The n value indicates that the crystallization is diffusion controlled, with decreasing nucleation rate. Scanning electronic microscopy showed the presence of nanoparticulated powder.

Keywords: *BZN, pyrochlore, Avrami, kinetic*

1. Introduction

The advances in communication technology, especially in wireless communication systems, are improved by miniaturization of devices. Dielectric materials for such applications must have relatively large dielectric constant, low tangent loss (tanδ), small temperature coefficient of capacitance (TCC), and low firing temperature[1].

Pyrochlore and pyrochlore-related compounds occurring in the Bi_2O_3-ZnO-Nb_2O_5 (BZN) system has received special attention in the last years due to their high dielectric constants (ε), low dielectric losses, and compositionally tunable TCC. These properties, allied to low sintering temperatures (lower than 950 °C), make these compounds attractive candidates for applications in electrical systems, such as capacitors and high-frequency multilayer structures co-fired with metal electrodes[2].

The BZN system comprises two basic crystalline phases: a cubic-pyrochlore-structure with the composition $(Bi_{1.5}Zn_{0.5})(Zn_{0.5}Nb_{1.5})O_7$ (α-phase) and a low-symmetry-structure with the composition $Bi_2(Zn_{1/3}Nb_{2/3})_2O_7$ (β-phase). Their electrical properties are quite different (TCC is about –400 ppm/°C for the α-phase and +200 ppm/°C for the β-phase), which is an attractive feature in tunable temperature coefficient of capacitance devices[3].

In this paper, α-BZN nanopowder was synthesized by the polymeric precursor method, which is a chemical method based on the Pechini process[4] that has been successfully used for preparing several complex oxides[5-6]. The goal of this paper is to study, for the first time, the α-BZN kinetics crystallization, and to determine the kinetic parameters for the crystallization process. Based on kinetic parameters and XRD analysis, a mechanism for α-BZN crystallization was proposed.

*e-mail: gilmar@ita.br

2. Experimental

BZN powder (α phase) was synthesized by the polymeric precursors, based on the Pechini method, as already reported elsewhere[7-8]. The starting reagents were: bismuth oxide, Bi_2O_3 (99.99%, Aldrich), zinc acetate dehydrate, $(CH_3CO_2)_2Zn.2H_2O$ (99.5 %, Carlo Erba), and niobium ammonium oxalate, $NH_4H_2[NbO–(C_2O_4)_3].3H_2O$ (99.5% CBMM, Brazil). The resin was kept on a hot plate until a viscous gel was formed, which was thermally treated at 300 °C for 4 hours (named as α-BZN precursor). The samples were treated at 400, 500, 600, 700, and 900 °C for 2 hours in an electrical furnace. Crystalline phases were analyzed by X ray diffraction (XRD) using an INEL curved position-sensitive detector operating with CuKα radiation. The α-BZN precursor was analyzed by differential scanning calorimetry (DSC) at heating rates of 5, 10, 20, 25, 30 K/min using a NETZSCH STA404 equipment. The measurements were carried on using 20 mg sample mass in Al_2O_3 crucibles, under a 50 mL/min synthetic air flux. DSC data was treated by a deconvolution algorithm to produce two separated curves for each thermal event: the organic material decomposition and the α-BZN crystallization. The sample treated at 700 °C was evaluated by scanning electron microscopy (SEM) using a JEOL 6400 equipment.

3. Results

Figure 1 shows the crystalline phase evolution of α-BZN precursor treated at several temperatures. Samples treated at 300 °C are constituted only by an amorphous phase, at 400 °C it is verified the crystallization of the Bi_2O_3 phase, but the amorphous phase is still present. α-BZN was formed at 500 °C at expense of Bi_2O_3, which is

still present in the sample, and from 600 to 700 °C only the crystalline α-BZN pyrochlore phase is observed. Intermediary phases, such as $BiNbO_4$ or $Bi_5Nb_3O_{15}$ or a pseudo-orthorhombic pyrochlore phase, were not detected. From these results, one can conclude that at 600 °C the α-BZN crystallization process is completed, and α-BZN is the unique crystalline phase present in the sample.

Insert in the Figure 2 it is shown the DSC curve together with a thermogravimetric (TG) one. These curves were obtained at the same experimental conditions described in the experimental section at heating rate of 5 K/min. It is possible to observe in TG curve that the weight loss process occurs by an unique step in the temperature range of 330-760 °C. In this temperature range it can also be observed the presence of two exothermic peaks (principal and secondary ones). The principal peak must be related to most exothermic event and the secondary one occurs at the same temperature range observed to BZN crystallization in Figure 1. Hence it follows that the principal peak at DSC curve must be related to the oxidation process of the oxidation of organic materials and the secondary one must be related to BZN crystallization process. Figure 2 also shows the DSC curves of α-BZN precursor treated at 400 °C for 2 hours under several heating rate. The DSC results reveal two exothermic peaks: a major one, at around 500 °C, corresponding to the oxidation of organic materials, and a secondary one, at around 585 °C, corresponding to the crystallization process. These curves were treated by a deconvolution tool to isolate both events, and those curves related to the crystallization process are presented in Figure 3. The heating rate (ϕ) and the peak temperature (T_m) are inserted in the Figure 3, which shows that α-BZN crystallization occurs from 557 to 602 °C, depending on the heating rate, which is in accordance with XRD analysis.

Figure 4 shows the crystallized fraction (x) as a function of time (t) for each DSC heating rate curve, determined for each curve by Equation 1,

$$x = \frac{Area(T_0 \rightarrow T_i)}{Area(T_0 \rightarrow T_f)} \quad (1)$$

where: Area ($T_0 \rightarrow T_i$) is the peak area under the DSC curve from T_0 to some intermediate temperature (T_i), and Area($T_0 \rightarrow T_f$) is the total

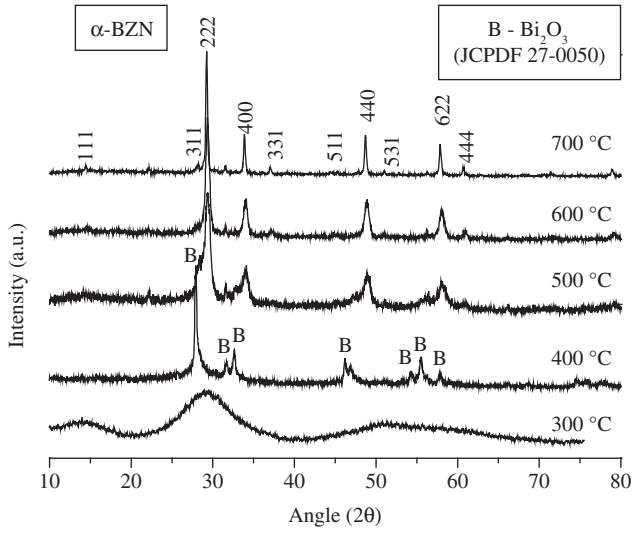

Figure 1. XRD patterns for the crystallization of α-BZN precursor. Samples were treated for 2 hours at indicated temperatures. B stands for Bi_2O_3.

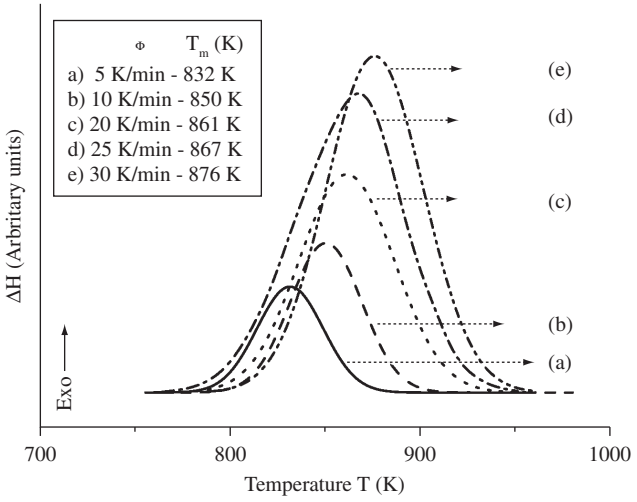

Figure 3. DSC curves related to the α-BZN crystallization.

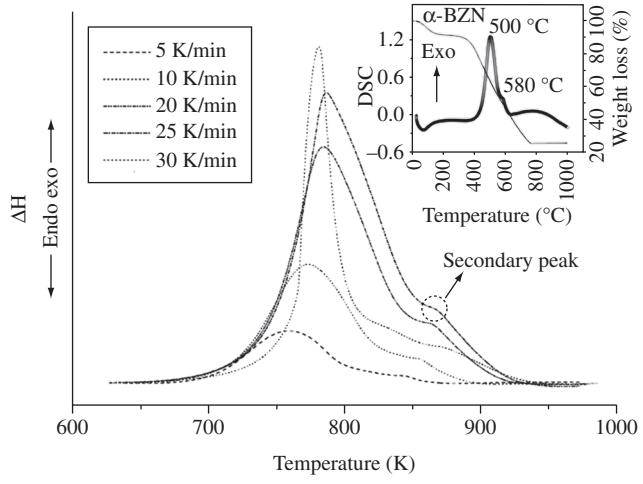

Figure 2. DSC curves of α-BZN precursor previously treated at 400 °C for 2 hours. The circle refers to the crystallization peak. The heating rates are indicated in the figure.

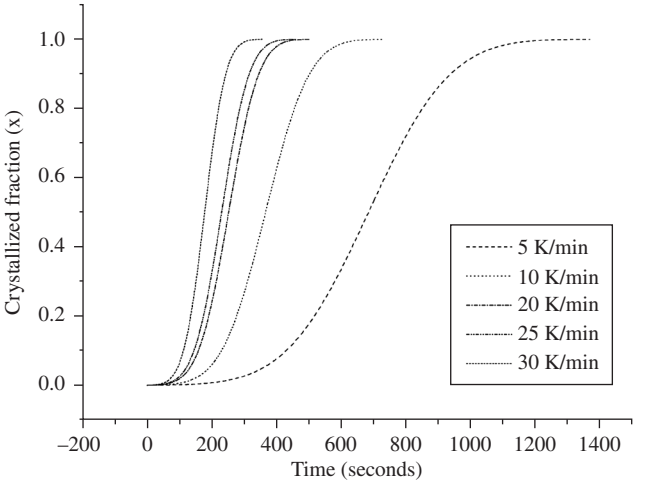

Figure 4. Crystallization fraction (x) for α-BZN crystallization at 5, 10, 20, 25, 30 K/min, under air flux.

area under the peak, both determined by numerical integration. The starting temperature, T_0, and the final temperature, T_f, were determined for each curve. T_0 is the temperature, in the increasing side, which corresponds to 0.25% of the ΔH peak height, and T_f is the temperature, in the decreasing side, which also corresponds to 0.25% ΔH peak height. They are related to initial time, T_0, and final time, T_f, respectively.

4. Discussion

4.1. Kissinger methodology

The Kissinger[9-11] methodology has been used to study the kinetic process of the non-isothermal crystallizations. This methodology is very simple, but it does not offer any information about Avrami's number and frequency factor. In order to verify the accuracy of Ligero method, the activation energy was determined from both: Kissinger and Ligero methods. The Kissinger methodology is illustrated in Equation 2. Where, ϕ is the heating rate, T_m is the DSC peak temperature, E is the activation energy, R is the gas constant and C is a constant. T_m and ϕ are taken from Figure 3; according to Equation 2 these values are used to make the plot in Figure 5. The linear adjustment gives the angular coefficient, which is used to determine the activation energy (E = 241 ± 24 kJ.mol^{-1}).

$$\ln\left(\frac{\varphi}{T_m^2}\right) = -\frac{E}{RT_m} + C \tag{2}$$

4.2. Ligero methodology

The Johnson-Mehl-Avrami-Kolmogorov[12-14] (JMAK) theory for isothermal crystallization is generally expressed by:

$$x = 1 - \exp[-(kt)^n] \tag{3}$$

where: x is the crystallized fraction, t the time, k the rate constant, and n the Avrami exponent. k is related to temperature by the Arrhenius equation:

$$k = k_o \exp\left(-\frac{E}{RT}\right) \tag{4}$$

where: k_0 is the frequency factor, E the activation energy, R the gas constant, and T the absolute temperature.

Taking the first derivative of x in relation to t in Equation 3:

$$\frac{dx}{dt} = (1-x)nk^n t^{n-1} \tag{5}$$

Eliminating the parameter t, the crystallization rate can be described as:

$$\frac{dx}{dt} = k(T)f(x) \tag{6}$$

These equations are derived for isothermal crystallization processes; nevertheless if ln[k_0f(x)], in Equation 7, is constant, they can be used for non-isothermal processes[15-16]. Substituting Equation 3 into Equation 5 and taking the logarithm, Equation (6) can be expressed by:

$$\ln\left(\frac{dx}{dt}\right) = \ln[k_0 f(x)] - \frac{E}{RT} \tag{7}$$

If k_0f(x) is a temperature independent constant there is a linear relationship between $\ln\left(\frac{dx}{dt}\right)$ and $\frac{1}{T}$. Consequently, E and k_0 can be determined.

As a first approximation, an arbitrary value of E is assumed and applied in Equation 7. From this equation k_0f(x) is determined for each pair (T, $\frac{dx}{dt}$). The temperature interval in which k_0f(x) remains constant with three significant digits is determined, obtaining a more accurate value for E. This reiterative process can be repeated several times and this procedure converges to a more and more accurate parameter E. In this work, the process was repeated three times, since the second and the third E values were the same. This procedure was carried out for each DSC curve giving the activation energy for the crystallization process for samples treated at 5, 10, 20, 25, and 30 K/min. Figure 6 shows a plot of $\ln\left(\frac{dx}{dt}\right)$ vs. $\frac{1}{T}$ after two reiterative processes, using data from the DSC curve obtained at 5 K/min.

The Avrami exponent (n) was determined by Equation 8[15-16], where x_1 and x_2 stands for pairs of c values which satisfy the conditions predicted by Equation 9[15-16].

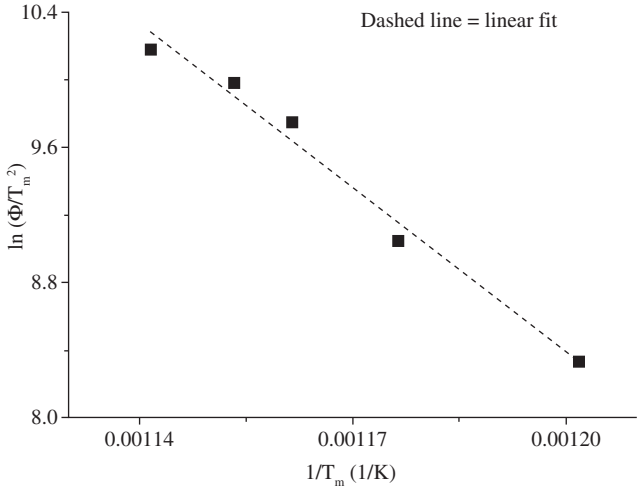

Figure 5. Kissinger plot for activation energy determination.

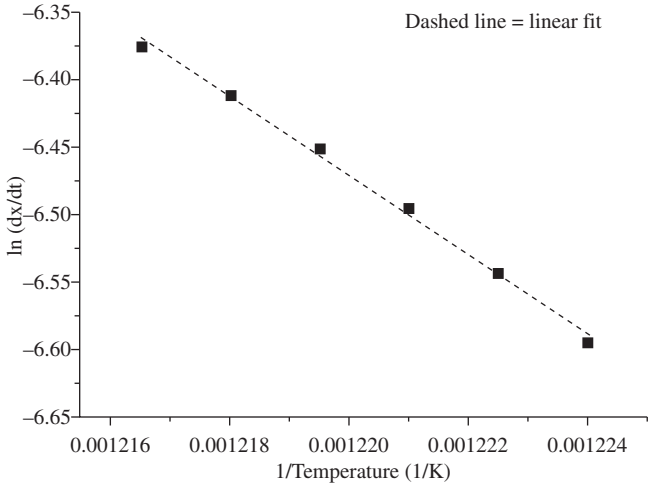

Figure 6. Arrhenius plot for DSC obtained at 5 K/min.

$$n = \ln\left[\frac{\ln(1-x_2)}{\ln(1-x_1)}\right]\left\{\ln\left[\frac{(1-x_2)\ln(1-x_2)}{(1-x_1)\ln(1-x_1)}\right]\right\}^{-1} \quad (8)$$

$$\ln[k_0 f(x_1)] = \ln[k\ f(x_2)] \quad (9)$$

Once n was obtained, Equation (10)[15-16] was used for k_0 determination.

$$C = \ln k_0 + \ln n + \ln(1-x) + \frac{n-1}{n}\ln[-\ln(1-x)] \quad (10)$$

C stands for the average value of the $\ln[k_0 f(x)]$.

Table 1 shows the activation energy(E) methods, the Avrami exponent (n), and the frequency factor (k_0) determined from each DSC curve, and the average values for α-BZN crystallization process. The average value of the activation energy determined from Ligero method and that determined from Kissinger method are also showed in the Table 1. One can observed that the activation energies determined from two completely different methods are very close.

The Avrami exponent average (n) is not an integer number. As suggested by Christian[17] it is an indication of a diffusion controlled process. In more details, Christian suggested that Avrami exponent in the range of 1 to 1.5 could be related to the diffusion controlled processes which mechanism has relation with the growth of particles with appreciable initial sizes.

According to Hu and Huang[18], in Bi–Zn–Nb–O cubic pyrochlores, the concentration of the oxygen vacancies seems to be the rate-controlling factor for grain growth, which indicates that the concentration of oxygen interstitial is the main factor for the diffusion process. Also, according to Wilde and Catlow[19] diffusion mechanism is responsible for the ionic conductivity of some pyrochlore oxides at high temperature and it is related to oxygen ion vacancy mechanism.

Figure 7 shows SEM images of α-BZN precursors treated for 2 hours at 700 °C. Even after this long thermal treatment, the images clearly reveal that the sample is composed of large agglomerated clusters, with dimensions of hundreds of nanometers. XRD analysis showed that α-BZN precursor calcined at 400 °C for 2 hours is constituted of highly crystalline Bi_2O_3 and an amorphous phase.

5. Conclusions

α-BZN has been synthesized by the Pechini method, and the kinetic parameters of crystallization have been determined. The crystallization process occurs at temperature as low as 600 °C. The activation energy determined from Ligero method was (242 ± 7) kJ.mol^{-1} and that determined from Kissinger method was (241 ± 24 kJ.mol^{-1}), the Avrami exponent was (1.3 ± 0.1), and the frequency factor was ~1x10^{13}.s^{-1}. The crystallization process is diffusion controlled.

Acknowledgements

The authors would like to acknowledge the support of CAPES and FAPESP.

Table 1. Activation energy, the Avrami exponent, and the frequency factor obtained from each DSC curve.

ϕ (K/min)	E (kJ.mol^{-1})	n	k_0 (seconds)
5	245 ± 10	1.3	~1 x 1013
10	239 ± 9	1.4	~1 x 1013
20	239 ± 9	1.2	~1 x 1013
25	242 ± 5	1.2	~1 x 1013
30	242 ± 5	1.2	~1 x 1013
Ligero average	242 ± 7	1.3 ± 0.1	~1 x 1013
Kissinger	241 ± 24	-	-

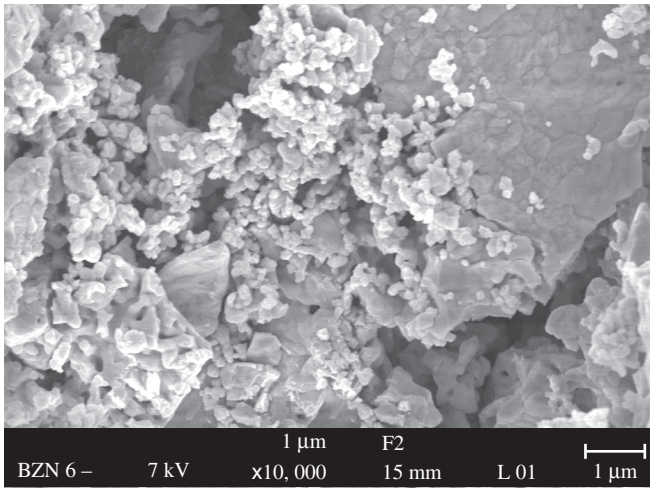

Figure 7. SEM image of α-BZN precursor treated at 700 °C for 2 hours.

References

1. Ren W, Trolier-McKinstry S, Randall CA, Shrout TR. Bismuth zinc niobate pyrochlore dielectric thin films for capacitive applications. *J. Appl. Phys*. 2001; 89(1):767-774.
2. Valant M, Davies PK. Synthesis and dielectric properties of pyrochlore solid solutions in the Bi_2O_3-ZnO-Nb_2O_5-TiO_2 system. *J. Mater. Sci*. 1999; 34(22):5437-5442.
3. Wei J, Zhang L, Yao X. Melting Properties of Bi_2O_3-ZnO-Nb_2O_5-Based Dielectric Ceramics. *J. Am. Ceram. Soc*. 1999; 82(9):2551-2552.
4. Pechini MP. Method of preparing lead and alkaline earth titanates and niobates and coating methods to form the capacitor. *US Patent* no. 3.330.697. 1967.
5. Zanetti SM, Leite ER, Longo E, Varela JA. $SrBi_2Nb_2O_9$ thin films deposited by dip coating using aqueous solution. *J. Eur. Ceram. Soc*. 1999; 19(6-7):1409-1412.
6. Zanetti SM, Bueno PR, Leite ER, Longo E, Varela JA. Ferroelectric and microstructural characteristics of $SrBi_2Ta_2O_9$ thin films crystallized by the RTA process. *J. Appl. Phys*. 2001; 89(6):3416-3420.
7. Zanetti SM, Silva SA, Thim GP. A chemical route for the synthesis of cubic bismuth niobate pyroclore nanopowders. *J. Solid State Chem*. 2004; 177:4546-4551.
8. Silva SA, Zanetti SM. Bismuth zinc niobate pyrochlore $Bi_{1.5}ZnNb_{1.5}O_7$ from a polymeric urea-containing precursor. *Mater. Chem. Phys*. 2005; 93(2-3):521-525.
9. Kissinger HE. Reaction Kinetics in Differential Thermal Analysis. *Analytical Chemistry*. 1957; 29(11):1702-1706.
10. Augis JA, Bennett JE. Calculation of the Avrami parameters for heterogeneous solid state reactions using a modification of the Kissinger method. *Journal of Thermal Analysis and Calorimetry*. 1979; 13(2):283-292.
11. Colmenero J, Barandiarán JM. Crystallization of $Al_{23}Te_{77}$ glasses. *Journal of Non-Crystalline Solids*. 1979; 30(3):263-271.
12. Avrami M. Kinetics of Phase Change. I: General Theory. *J. Chem. Phys*. 1939; 7(12):1103.
13. Avrami M. Kinetics of Phase Change. II: Transformation-Time relations for random distribution of nuclei. *J. Chem. Phys*. 1940; 8(2):212.
14. Avrami M. Kinetics of Phase Change. III: Granulation, Phase Change an Microstructures. *J. Chem. Phys*. 1941; 9(2):177.
15. RLigero A. A study of the crystallization kinetics of some Cu-As-Te glasses. *J. Mat. Sci*. 1991; 26(1):211-215.
16. Campos AL, Silva NT, Melo FCL, Oliveira MAS, Thim GP. Crystallization kinetics of orthorhombic mullite from diphasic gels. *J. Non-Cryst. Solids*. 2002; 304(1-3):19-24.
17. Christian JW. *The theory of transformations in metals and alloys*. New York: Pergamon Press; 1995. p. 542.
18. Hu Yi, Huang CL. Structural characterization of Bi–Zn–Nb–O cubic pyrochlores. *Ceramics International*. 2004; 30(8):2241-2246.
19. Wilde PJ, Catlow CRA. Defects and diffusion in pyrochlore structured oxides. *Solid State Ionics*. 1998; 112(3-4):173-183.